ACCEPTED MANUSCRIPT

Investigation of backwashing effectiveness in membrane bioreactor (MBR) based on different membrane fouling stages

Zhao Cui[a], Jie Wang[a]*, Hongwei Zhang[a], Huu Hao Ngo[b], Hui Jia[a], Wenshan Guo[b] Fei Gao[c] and Guang Yang[c]

[a] State Key Laboratory of Separation Membranes and Membrane Processes, Tianjin Polytechnic University, Tianjin, 300387, China

[b]School of Civil and Environmental Engineering, University of Technology Sydney, Australia

[c] School of Environmental Science and Engineering, Tianjin University, Tianjin 300072, China

* Corresponding author:

1. email: wangjiemailbox@163.com (Jie Wang)

Tel.: +86 022 8395 5668;

ACCEPTED MANUSCRIPT

ACCEPTED MANUSCRIPT

Abstract

In this study the effect of different fouling stages of hollow fiber membranes on effective backwashing length in MBR has been investigated. Computational fluid dynamics (CFD) is imported to simulate backwashing process. A multi-physics coupling model for free porous media flow, convective mass transfer and diluted species transport was established. The laser bijection sensors (LBS) were imported to monitor the backwashing solution position inside fiber lumen. Simulation results indicated that membrane fouling degree could change the velocity of backwash solution inside fiber lumen and make a further effect on effective backwash length. The signal variations of LBS are in accordance with the simulation results. The backwashing process can only play an active role when the filtration pressure is below the critical TMP. It can be concluded that backwash duration in industrial applications need to be set based on changes in TMP.

Keywords: Membrane bioreactor (MBR); Membrane backwashing; Hollow fiber length; CFD simulation; Laser bijection sensors

ACCEPTED MANUSCRIPT

ACCEPTED MANUSCRIPT

1. Introduction

Membrane bioreactor (MBR) is an attractive process in space limited areas by replacing the secondary sediment tank for the purpose of separation of water and biomass in wastewater treatment due to its small footprint (Fan et al., 2018; Shen et al., 2015; Yang et al., 2017). Nevertheless, they are usually suffered the problem of membrane fouling, leading to: firstly, an increase in TMP (transfer membrane pressure) under constant flux conditions; and secondly, a dramatic drop in the permeate flux under constant pressure conditions (Miller et al., 2014; Rajesh Banu et al., 2009; Takada et al., 2018).

As for MBR membrane fouling control, the main factors have been reported (Lin et al., 2014; Shen et al., 2015; Yu et al., 2014) as: operations (aeration, bubble diameter, HRT, flux, SRT, addition of powdered activated flocculants or carbon), activated sludge conditions (including MLSS, viscosity, particle diameter, F/M, rheology, SMP, EPS, zeta potential, surface tensions), configuration (reactor, membrane module) and membrane materials (membrane structure, hydrophilicity, hydrophobicity). Hydrodynamics plays an important role in reversible fouling control which contains cake layer detachment and bio-solids migration(Wang & Wu, 2009). Computational fluid dynamics (CFD) as a powerful tool can systematical analysis the effect of hydrodynamics on reversible fouling(Meister et al., 2018). Xie (Xie et al., 2018) investigated the effect of a micro-channel turbulence promoter installation on the hydrodynamic performance of a submerged membrane bioreactor. CFD simulation results and the experimental results showed that the enhancement effect of SMBR equipped with MCTP in the vertical orientation was better than that of SMBR equipped with MCTP in the horizontal orientation. Yang (Yang et al., 2017) investigated the reversible membrane fouling control according to cake layer formation and foulants deposition in MBR by the combination of CFD and design of experiment. The results

ACCEPTED MANUSCRIPT

indicated that sludge concentration is the key influencing factor comparing with sludge viscosity and strain rate, particle deposition propensity and shear stress. A medium sludge concentration of 8820 mg/L is optimal for the reversible fouling reduction. The bubble diameter is more decisive than air flowrate for membrane shear stress due to its role in sludge viscosity. Yang (Yang et al., 2016) also developed a CFD model incorporating sub-models of oxygen transfer, bio-kinetics and sludge rheology for the cost optimization of a bench-scale MBR. The results indicated that the optimized height of gas-liquid dispersion was at around 300 mm. The model also showed that the high nitrogen removal efficiency was obtained due to the high recirculation rate driven by airlift force without destroying the oxygen enrichment and deprivation in the oxic and anoxic zone, respectively. These strategies all contribute to helping us understand the methods in mitigating the membrane fouling in filtration process. But there is almost no research on membrane backwashing in MBR system which was seemed as the departure point of this study.

Backwashing as an effective membrane control method has been reported to successfully remove fouling deposits and is particularly convenient as a part of a dead-end hollow fiber filtration cycle(Cui et al., 2017; Cui et al., 2018). Previous studies focused on the intensity, optimal backwash frequency, duration and air sparging to improve backwash efficiency (De Sotto et al., 2018; Shekhar et al., 2017; Yigit et al., 2009). The aim of a series of tests in this study is to investigate the effect of dynamic change of membrane fouling on effective backwashing length in MBR system with the evolution software of CFD. A multi-physics coupling model for free porous media flow, convective mass transfer and diluted species transport was established and the results are verified with experimental studies. The laser bijection sensors (LBS) were installed in each piece of membrane aimed to monitor the backwashing solution position inside

ACCEPTED MANUSCRIPT

the fiber lumen. The dynamic changes of fouling resistance (R_f) and membrane resistance (R_m) was simulated as well as experimental verification. The comparison of the simulated and experimental results was hoped to provide a theoretical basis on the effective backwashing in MBR systems.

2 Methodology

2.1 Model description

Model parameters, Detailed simulation steps, post-processing steps and solution methods will be discussed in the following sections. Positive pressure hollow fiber membranes were used as the research object, mainly investigated the fluid behavior inside the fiber lumen under a transient flow condition with the dead-end backwashing modes. A multi-physics coupling model for free porous media flow, convective mass transfer and diluted species transport was established. Further, the fluid is assumed to be Newtonian, incompressible, isothermal and having constant physical properties under steady state conditions (Kaya et al., 2014). The diffusivity is chosen as the constant fluid property shown in Tab. 3. The reason for choosing these assumptions is to avoid the effects of flow state on mass transfer under short duration conditions and simplify calculation.

The flow state (laminar or turbulence flow) was determined by the Reynolds number (R_e). The fluid will exhibit different flow regimes, pressures, and velocity profiles with different R_e numbers, forming different boundary layers and wakes. The R_e is shown in Eq. (1):

$$R_e = \frac{\rho U L}{\mu} \tag{1}$$

Where ρ is fluid density; U is characteristic flow rate; L is feature length; μ is dynamic viscous coefficient.

R_e number is a dimension that characterizes the relative ratio of viscous and inertial

ACCEPTED MANUSCRIPT

forces during fluid motion. Because the flow velocity and characteristic scale of the hollow fiber membrane filament are small, it can be considered that the fluid in the calculation domain is in a laminar flow state.

2.1.1 Free porous media flow model

The fluid in the calculation domain is a laminar, incompressible fluid. The hollow fiber membrane is regarded as a porous medium. Darcy's law is summarized as shown in Eq. (2):

$$q_v = -K\frac{dh}{dl} \tag{2}$$

Where K is permeability coefficient; dh/dl is hydraulic gradient. The relationship shows that the velocity of fluid permeation through the porous medium per unit time is proportional to the hydraulic gradient and the permeability.

During the membrane backwashing process, the velocity of flow inside the hollow fiber are slow. The flow is a laminar flow state which conforms to the conditions of Darcy's law. Thus, the relationship between backwashing flux and transmembrane pressure (TMP) is shown in Eq. (3):

$$\mathrm{J} = \frac{\Delta P}{\mu(R_m + R_f)} \tag{3}$$

Where J is membrane backwashing flux; ∇P is transmembrane pressure; R_m is the membrane resistance; R_f is the resistance of fouling layer. Then the backwashing flow (Q) could be calculated as Eq. (4) (Wang et al., 2014):

$$\mathrm{Q} = \pi D_i \int_0^l J\, dx \tag{4}$$

Where Di is inner diameter of hollow fiber; l is effectiveness backwashing length. The effective backwashing length is defined as the valid backwashing fiber axial range that the backwashing flow can take into effect.

The free porous media flow model combines the Stokes-Einstein equation describing

ACCEPTED MANUSCRIPT

the fluid flow with the Boltzman equation describing the permeate flow in porous media. This combination of fluid flow is constant with the actual fluid flow inside the hollow fiber membrane lumen which can better represent the flow of liquid within the membrane. The equation for calculating the fluid flow in the inner membrane surface is mass conservation equation and Stokes-Einstein equation:

$$\nabla\vec{U} = 0 \tag{5}$$

$$\frac{\partial\vec{U}}{\partial t} + (\vec{U}\cdot\nabla)\vec{U} = -\frac{1}{\rho}\nabla P + \mu\nabla^2\vec{U} \tag{6}$$

Where $\vec{U}$ is velocity vector for the fluid. The Boltzman equation is an extension of Darcy's law. The flow equation of porous media in the computational domain is as follows:

$$\frac{\rho}{\varepsilon_p}\left[(\vec{U}\cdot\nabla)\frac{\vec{U}}{\varepsilon_p}\right] = \nabla\cdot\left\{-PI + \frac{\mu}{\varepsilon_p}\left[\nabla\vec{U} + \nabla\vec{U}^T\right] - \frac{2\mu}{3\varepsilon_p}(\vec{U}\cdot\nabla)I\right\} - \left(\frac{\mu}{K_{br}} + \beta_F|\vec{U}| + \frac{Q_{br}}{{\varepsilon_p}^2}\right) \tag{4}$$

Where ε_p is porosity; I is unit tensor; K_{br} is permeability; β_F is the coefficient related to the nature of porous media; Q_{br} is permeation amount within the calculation area and the value is $\rho\nabla\cdot\vec{U}$.

2.1.2 Convective mass transfer

Convective mass transfer refers to mass transfer between a fluid and a solid wall, or mass transfer between moving fluids which are immiscible and separated by a moving interface. Therefore, the convective mass transfer is related not only to the dynamic properties of the moving fluid but to the nature of the transmissive component. Convection is subdivided into natural convection and forced convection: it is called natural convection if the fluid motion is caused by the difference in solution density; it is called forced convection if the fluid is caused by external forces. The convective mass transfer can be expressed as:

$$N = K_c\Delta C \tag{7}$$

ACCEPTED MANUSCRIPT

Where N is mass transfer flux for the diffusion component; K_c is convective mass transfer coefficient; ΔC is the concentration difference between the mainstream concentration of the diffusion component and the boundary surface concentration.

2.1.3 Diluted species transport

The diluted species transport model is to study the convective diffusion phenomenon of substances in the computational domain. For the mass transfer of raw water foulants in the model calculation domain, it is considered that the diluted species transport model can be coupled with the free porous medium flow model if the solute concentration is less than 10%. The foulants trapped and accumulated in the membrane surface during membrane filtration process (much higher than 10%) are treated as porous media which are similar to membranes.

The dilute substance transfer control equation is as follows:

$$\nabla(D\nabla C) + \hat{U}(\nabla C) = 0 \tag{8}$$

Where D is diffusion coefficient for foulants; ∇C is for solution concentration; $\hat{U}$ is the velocity field calculated from the free porous media flow equation.

Fick's law provides methods for studying solute and solution diffusion phenomena. While the dilute substance transfer model can be combined with the velocity field to provide convection diffusion research methods for dilute substances.

2.2 Geometric model establishment and parameter selection

To verify the accuracy of the CFD solution, a mesh independence study was carried out. Fig. 1 illustrate the channel and geometry used in this paper. As shown in the figure, area I is the internal flow area of the membrane, area II is the porous medium area, and area III is fouling layer area. Boundary condition settings were shown in Tab. 1 and Tab. 2.

The parameters used in backwashing process were shown in Tab. 3.

ACCEPTED MANUSCRIPT

The final discretisation mesh contained at least 25 elements within an inflation layer normal to all solid bound-aries. The thickness is equal to approximately 2% of the channel height as well as the channel height of non-structured elements within a maximum size of 1%. The mesh consists half a million elements whose Grid Convergence Index is lower than 5% for both mass transfer and permeate flux. It indicated that the mesh resolution is within an acceptable range, and that this potential source of the numerical error can be safely neglected (Lim et al., 2018).

2.3 Experimental validations

The pilot-scale MBR shown in Fig. 2, was completed in May 2017 at a wastewater treatment plant in Beijing and was operated for over 365 days with a filtration flux of 35 LMH as well as the capacity of 500 m^3/d. The MLSS of the sludge is 12000 mg/L. Sludge is removed every day after the installation starts was well as the sludge kept at 35d. A system designed for the pilot-scale operations is used to control the operation of the MBR system. Hollow fiber membranes used in this MBR were made of PVDF (pore size of 0.2 μm) which was supported by membrane frames.

Fouled membranes module (1.8m) in MBR system was cut down to conduct with the backwashing operation (Cui et al., 2018). The bench-scale experiments were shown in Fig. S1. In this study, the 1.8 m membrane fiber was cut into several pieces. The LBSs were installed in each piece of membrane aimed to monitor the backwashing solution position inside the fiber lumen. The signals will be transferred directly to the computer by the data acquisition card. The principle of laser measurement for membrane backwashing is based on the light propagation in different medium (Cui et al., 2018).

2.4 Design of fouling experiments

In this study, the flux of virgin membrane when filtrating tap water was 35m^3/h with

ACCEPTED MANUSCRIPT

the TMP of 0.01Mpa. Here, the TMP was imported as a standard for evaluating the resistance of membrane and fouling layer. The resistance of fouling layer was 0.01Mpa with the water production of 35m^3/h. Thus, the degree of membrane fouling experiments design were shown in Tab. 4. In the MBR system, the critical TMP is 0.05 MPa. Thus, the fouling stages were classified as follows: Initial fouling stage was defined as the stage in which membrane fouling resistance (R_f) is less that membrane resistance (R_m); Mid-term fouling stage was defined as the stage in which R_f is higher than R_m but less than the critical TMP; Late fouling stage was defined as the stage in which R_f is higher than the critical TMP. The fouling layer here was seemed as the super concentrated solution. The fouling layer density was calculated as:

$$\rho_m = \frac{m}{V} \tag{9}$$

$$V = \pi(r_f^{\,2} - r_o^{\,2})^2 L_m \tag{10}$$

Where ρ_m is fouling layer density; m is the quality of foulants on the membrane surface; V is fouling layer volume; r_f is the radius of the fouling layer; r_o is outer radius of hollow fiber. The thickness of fouling layer here was measured as 22μm, 42μm and 65μm respectively when filtration TMP reached to 0.015Mpa, 0.02Mpa and 0.05Mpa by ultrasonic spectrum analysis. Thus, the density of foulants was calculated by Eq. (9) and (10) with weighing method. The calculated fouling layer densities were shown in Tab. 4 as 10000, 15000 and 50000mg/L.

3 Results and discussion

3.1 Simulation of effective backwash length under different Fouling degrees

Differing from the current CFD simulation studies which focus on the optimization of the whole membrane reactor (Wu et al., 2018; Yang et al., 2017), this study held a microscopic point of view. Mainly simulated the fluid behavior in a single membrane fiber in order to provide some guidance for backwashing process.

ACCEPTED MANUSCRIPT

3.1.1 Backwash length simulation at initial membrane fouling stage

In this section, the velocity inside fiber lumen with the fouling layer thickness of 22μm was shown in Fig. 3. As it can be seen, the position of the flow velocity inside lumen arrived at 179.25 cm after 0.01 seconds of backwashing. It can be considered that the backwashing solution reached the position of 0.75 cm from the inlet. When the backwashing is conducted for 0.8s, the variation of flow velocity reached to 59.9 cm which was constant with the position of backwashing solution. After the backwashing process was conducted for 1.61s, the flow rate change position reached 120.1cm as well as final position of the flow rate inside the fiber stayed at 120.2cm. This result indicated that the effective backwashing length of 1.8m membrane was only 1.2m when the fouling resistance was less than membrane resistance. The reason may be that selective permeation of backwashing solution limited the delivery of backwashing solution to the far end of a long fiber (Cui et al., 2018).

3.1.2 Backwash length simulation at mid-term membrane fouling stage

Keep other simulation conditions unchanged and only change the fouling layer thickness to 42μm. Then the simulation results were shown in Fig. 4. As shown in the figure, the position of the flow velocity inside lumen arrived at 0.95 cm after 0.01 seconds of backwashing which was faster than that of Fig. 3. When the backwashing is continued for 0.8s, the variation of flow reached to 75.9 cm. As the backwashing conducted, the position of the flow rate inside the fiber arrived at 150.2 cm at 1.57s. And final position of the flow rate inside the fiber stayed at 150.4 cm, too. The results indicated that the degree of membrane fouling could change the velocity of backwash solution inside fiber lumen which would further change the effective backwash length. The higher the degree of membrane fouling, the longer the effective backwashing length.

ACCEPTED MANUSCRIPT

3.1.3 Backwash length simulation at late membrane fouling stage

In this section, other simulation conditions were kept the same and only increased the fouling layer thickness to 65μm. As shown in Fig. 5, the position of the flow velocity inside lumen arrived at 1.18 cm after 0.01 seconds of backwashing which was faster than that of Fig. 3 and Fig. 4. When the backwashing is continued for 0.8s, the variation of flow velocity reached to 94. 5 cm as well as the finally position of 171.2 cm. These results indicated that the degree of fouling determines the effective backwashing length under the premise fixed backwashing flow.

3.2 Verification experiments of effective backwash length

The verification experiments were conducted in this section and experimental design follows section 2.4. In order to avoid errors caused by uneven fouling, each set of experimental data is obtained by verifying different membrane fibers on the same membrane module for more than 5 times.

Firstly, the backwashing process started when the filtration TMP increased to 0.015MPa at the initial membrane fouling stage. The backwashing velocity offered by piston pump was 1.2 m/s. As it can be seen in Fig. 6(a), the signal of monitoring point (MP) 1 changed from 0 to 1 at 1.52s which meant that backwashing solution had traveled 1.2 m inside fiber lumen within 1.52s. Then looking at the signals of MP 2 to 4, there were no signal variations in the whole backwashing duration of 60s. It indicated that there was no backwashing solution passed these monitoring points. The effective backwashing length is 1.2 m when backwashed at initial membrane fouling stage.

Secondly, the backwashing process started when the filtration TMP increased to 0.02 MPa the backwashing process started when the filtration TMP increased to 0.015MPa at the mid-term membrane fouling stage. As it can be seen in Fig. 6(b), the signal of MP 1 changed from 0 to 1 at 1.22s which meant that backwashing solution had traveled

ACCEPTED MANUSCRIPT

1.2 m inside fiber lumen within 1.22s. It is obvious that the velocity of backwashing solution inside fiber lumen was higher than that of Fig. 6(a). The limited velocity revealed by LBS could be attributed to the outflow flux of backwashing solution in axial direction, which dissipates the driving force (pressure) of the cleaning solution further to the longer distance along the hollow fibers. Meanwhile, the signal of MP2 changed from 0 to 1 at the moment of 1.43s. No signal variations in the whole backwashing duration of 60s in MP 3 and 4. It indicated that the effective backwashing length is 1.4 m when backwashed at mid-term membrane fouling stage.

Finally, the backwashing process started when the filtration TMP increased to 0.05 MPa the backwashing process started when the filtration TMP increased to 0.015MPa at the late membrane fouling stage. As it can be seen in Fig. 6(c), the signal of MP 1 changed from 0 to 1 at 1.04s whose velocity of backwashing solution inside fiber lumen was higher than that of Fig. 6(a) and (b). Meanwhile, the signal of MP2 changed from 0 to 1 at the moment of 1.22s as well as the signal of MP3 changed at 1.39s. But, there are still no signal variations in the whole backwashing duration of 60s in MP4. It indicated that the effective backwashing length is 1.6 m when backwashed at late membrane fouling stage. The severe the membrane fouling is corresponded to the higher velocity inside the lumen and the longer effective backwash length.

To further verify the results accuracy, the flux recovery rates of Fig. 6 were shown in Tab. 5. The operating condition was the same as mentioned in section 2.3. As it can be seen that long effective backwash length does not correspond to high backwash efficiency. The backwashing process can only play an active role when the filtration pressure is below the critical TMP. It can be concluded that backwash cycles in industrial applications need to be set based on changes in TMP.

3.3 Comparison of simulation and experimental results

ACCEPTED MANUSCRIPT

The results of simulation and experiment were compared in this section. The backwashing durations at different fouling stages with different backwashing lengths were shown in Tab. 6. At the stage of $R_f < R_m$, the effective backwashing length was only 120cm with the deviation of 0.053. As the fouling degree increased to $Rf \geq Rm$, the effective backwashing length increased to 140cm with the deviation from 0.045 to 0.049. When operated at the stage of Rf >> Rm, the effective backwashing length increased to 160cm with the deviation from 0.122 to 0.125. The deviation was calculated as below:

$$\sigma = \frac{|V_e - V_s|}{V_e} \tag{11}$$

where σ is deviation; V_e is experimental value; V_s is simulation value. It supports the fact that the simulation results are in good agreement with the experimental data.

4 Conclusion

Different fouling stages to effective backwashing length in MBR was investigated with CFD simulation. A multi-physics coupling model for free porous media flow, convective mass transfer and diluted species transport was established. Conclusions are as follows:

(1) Simulation results showed that membrane fouling degree could affect the velocity of backwash solution inside fiber lumen and then change effective backwash length.

(2) The signal variations of LBS are in accordance with simulation results. But, long effective backwash length does not correspond to high backwash efficiency.

(3) Backwash duration in industrial applications needs to be set according to the changes of TMP.

Nomenclature

ACCEPTED MANUSCRIPT

R_e Reynolds number

ρ fluid density, kg/m^3

U characteristic flow rate, m/s

L feature length, m

μ dynamic viscous coefficient, kg/m·s

q_v velocity of fluid permeation through the porous medium

K permeability coefficient

dh/dl hydraulic gradient

J membrane backwashing flux, L/m^2h

∇P transmembrane pressure, kPa

R_m the membrane resistance, kg/m^2

R_f resistance of fouling layer, kg/m^2

Q backwashing flow, L/h

l effectiveness backwashing length, m

$\vec{U}$ velocity vector for the fluid, m/s

∇P pressure gradient, KPa

ε_p porosity

I unit tensor

K_{br} permeability, %

β_F the coefficient related to the nature of porous media

Q_{br} permeation amount within the calculation, m^3/h

N mass transfer flux for the diffusion component, L/m^2h

K_c convective mass transfer coefficient

ΔC difference between the boundary surface concentration and the mainstream concentration of the diffusion component, mg/L

ACCEPTED MANUSCRIPT

ACCEPTED MANUSCRIPT

D diffusion coefficient for foulants, m^2/s

∇C solution concentration, mg/L

$\hat{U}$ velocity field calculated from the free porous media flow equation, m/s

ρ_m fouling layer density, mg/L

m quality of foulants on the membrane surface, mg

V fouling layer volume, L

r_f radius of the fouling layer, m

r_o outer radius of hollow fiber, m

Acknowledgments

This study was financially supported by the National Natural Science Foundation of China (No.51578375. No.51638011), China Postdoctoral Science Foundation (2017M621081), Program for Changjiang Scholars and Innovative Research Team in University of Ministry of Education of China (Grand No. IRT-17R80). The research collaboration between Tianjin Polytechnic University and University of Technology Sydney is grateful. We also thanks for the support of China Scholarship Council (No. 201609345007, No. 201709345009).

References

Cui, Z., Wang, J., Zhang, H., Jia, H. 2017. Influence of released air on effective backwashing length in dead-end hollow fiber membrane system. *Journal of Membrane Science*, **530**, 132-145.

Cui, Z., Wang, J., Zhang, H., Song, L., Jia, H., Yang, G., Gao, F. 2018. Influence of selective permeation of backwashing solution on the cleaning effectiveness in hollow fiber system. *Journal of Membrane Science*, **546**, 139-150.

De Sotto, R., Ho, J., Lee, W., Bae, S. 2018. Discriminating activated sludge flocs from biofilm microbial communities in a novel pilot-scale reciprocation MBR using high-throughput 16S rRNA gene sequencing. *Journal of Environmental Management*, **217**, 268-277.

Fan, H., Xiao, K., Mu, S., Zhou, Y., Ma, J., Wang, X., Huang, X. 2018. Impact of membrane pore morphology on multi-cycle fouling and cleaning of hydrophobic and hydrophilic membranes during MBR operation. *Journal of Membrane Science*, **556**, 312-320.

Kaya, R., Deveci, G., Turken, T., Sengur, R., Guclu, S., Koseoglu-Imer, D.Y., Koyuncu, I. 2014. Analysis of wall shear stress on the outside-in type hollow fiber membrane modules by CFD simulation. *Desalination*, **351**, 109-119.

Lim, S.Y., Liang, Y.Y., Fimbres Weihs, G.A., Wiley, D.E., Fletcher, D.F. 2018. A CFD study on the effect of membrane permeance on permeate flux enhancement generated by unsteady slip velocity. *Journal of Membrane Science*, **556**, 138-145.

Lin, H., Zhang, M., Wang, F., Meng, F., Liao, B.-Q., Hong, H., Chen, J., Gao, W. 2014. A critical review of extracellular polymeric substances (EPSs) in membrane bioreactors:

ACCEPTED MANUSCRIPT

Characteristics, roles in membrane fouling and control strategies. *Journal of Membrane Science*, **460**, 110-125.

Meister, M., Rezavand, M., Ebner, C., Pümpel, T., Rauch, W. 2018. Mixing non-Newtonian flows in anaerobic digesters by impellers and pumped recirculation. *Advances in Engineering Software*, **115**, 194-203.

Miller, D.J., Kasemset, S., Paul, D.R., Freeman, B.D. 2014. Comparison of membrane fouling at constant flux and constant transmembrane pressure conditions. *Journal of Membrane Science*, **454**, 505-515.

Rajesh Banu, J., Uan, D.K., Yeom, I.-T. 2009. Nutrient removal in an A2O-MBR reactor with sludge reduction. *Bioresource Technology*, **100**(16), 3820-3824.

Shekhar, M., Shriwastav, A., Bose, P., Hameed, S. 2017. Microfiltration of algae: Impact of algal species, backwashing mode and duration of filtration cycle. *Algal Research*, **23**, 104-112.

Shen, L.-g., Lei, Q., Chen, J.-R., Hong, H.-C., He, Y.-M., Lin, H.-J. 2015. Membrane fouling in a submerged membrane bioreactor: Impacts of floc size. *Chemical Engineering Journal*, **269**, 328-334.

Takada, K., Hashimoto, K., Soda, S., Ike, M., Makio, T., Nakayama, Y., Miyamoto, H., Yamashita, K., Hashimoto, T. 2018. Microbial Communities on the Submerged Membranes in Full-Scale Membrane Bioreactors Treating Municipal Wastewater. *Journal of Environmental Engineering*, **144**(1), 04017084.

Wang, J., Cui, Z., Jia, H., Zhang, H. 2014. The effect of fiber length on non-uniform and hysteresis phenomenon in hollow fiber membrane backflushing. *Desalination*, **337**, 98-108.

Wang, Z., Wu, Z. 2009. A Review of Membrane Fouling in MBRs: Characteristics and Role of Sludge Cake Formed on Membrane Surfaces. *Separation Science and Technology*, **44**(15), 3571-3596.

Wu, Q., Yan, X., Xiao, K., Guan, J., Li, T., Liang, P., Huang, X. 2018. Optimization of membrane unit location in a full-scale membrane bioreactor using computational fluid dynamics. *Bioresource Technology*, **249**, 402-409.

Xie, F., Ge, H., Liu, J., Chen, W., Song, H. 2018. CFD and experimental studies the effect of micro-channel turbulence promoter installation on the hydrodynamic performance of submerged flat-sheet membrane bioreactor. *Chemical Engineering and Processing - Process Intensification*, **127**, 28-35.

Yang, M., Wei, Y., Zheng, X., Wang, F., Yuan, X., Liu, J., Luo, N., Xu, R., Yu, D., Fan, Y. 2016. CFD simulation and optimization of membrane scouring and nitrogen removal for an airlift external circulation membrane bioreactor. *Bioresource Technology*, **219**, 566-575.

Yang, M., Yu, D., Liu, M., Zheng, L., Zheng, X., Wei, Y., Wang, F., Fan, Y. 2017. Optimization of MBR hydrodynamics for cake layer fouling control through CFD simulation and RSM design. *Bioresource Technology*, **227**, 102-111.

Yigit, N.O., Civelekoglu, G., Harman, I., Koseoglu, H., Kitis, M. 2009. Effects of various backwash scenarios on membrane fouling in a membrane bioreactor. *Desalination*, **237**(1), 346-356.

Yu, H., Lin, H., Zhang, M., Hong, H., He, Y., Wang, F., Zhao, L. 2014. Membrane fouling in a submerged membrane bioreactor with focus on surface properties and interactions of cake sludge and bulk sludge. *Bioresource Technology*, **169**, 213-219.

ACCEPTED MANUSCRIPT

ACCEPTED MANUSCRIPT

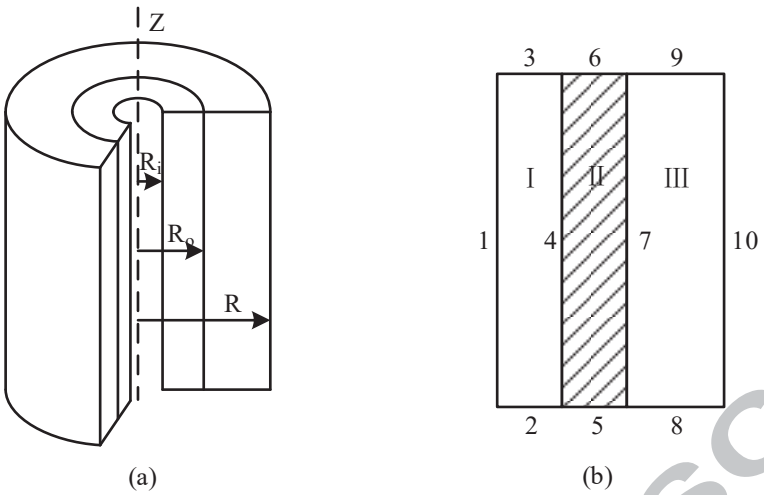

Fig. 1 Geometric model of hollow fiber membrane: (a) Spatial model; (b) 2D axisymmetric model

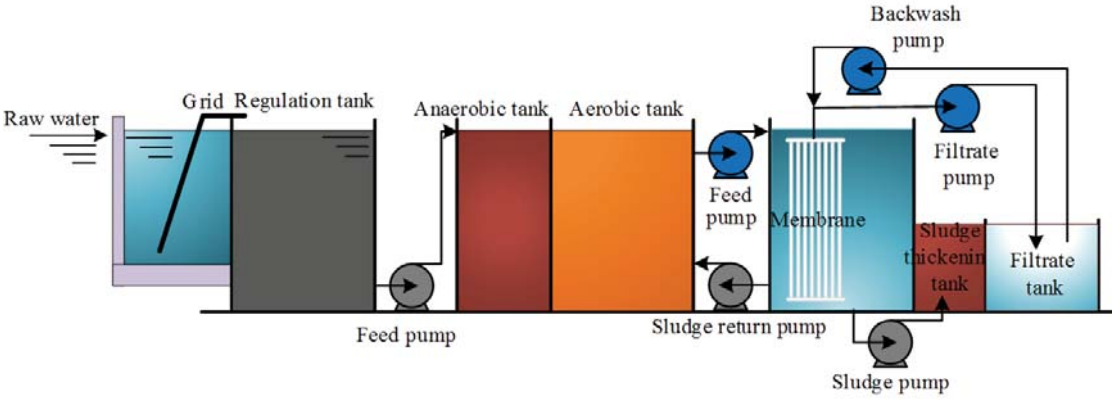

Fig. 2 Schematic diagram of the pilot scale MBR system

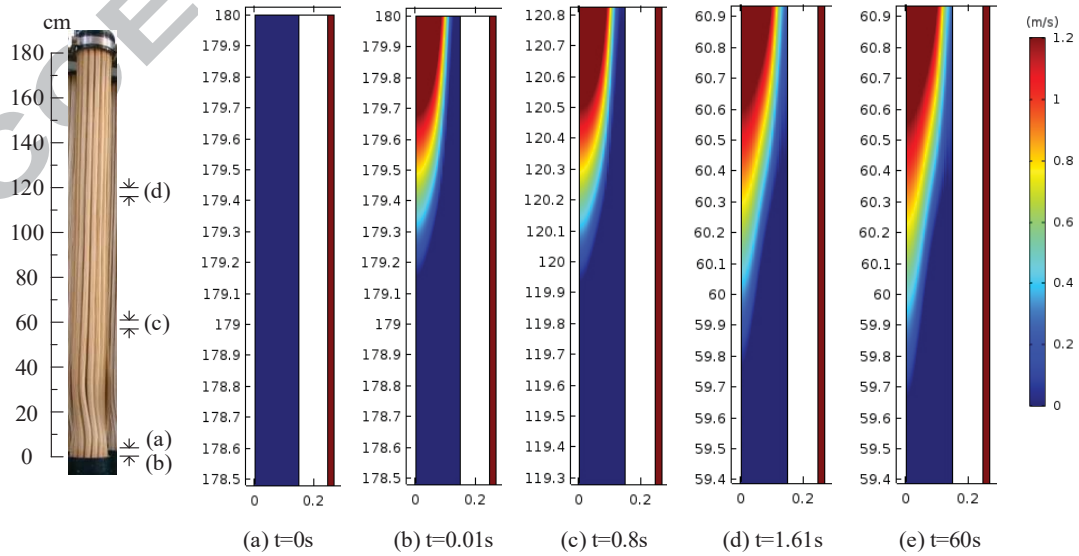

(a) t=0s (b) t=0.01s (c) t=0.8s (d) t=1.61s (e) t=60s

ACCEPTED MANUSCRIPT

Fig. 3 Velocity variation inside fiber lumen at initial membrane fouling stage

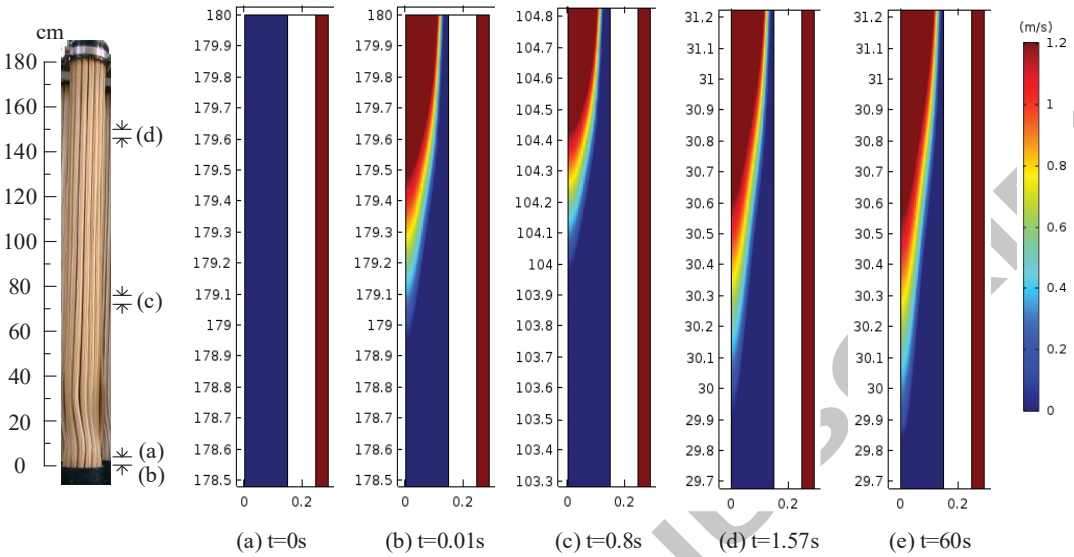

Fig. 4 Velocity variation inside fiber lumen at mid-term membrane fouling stage

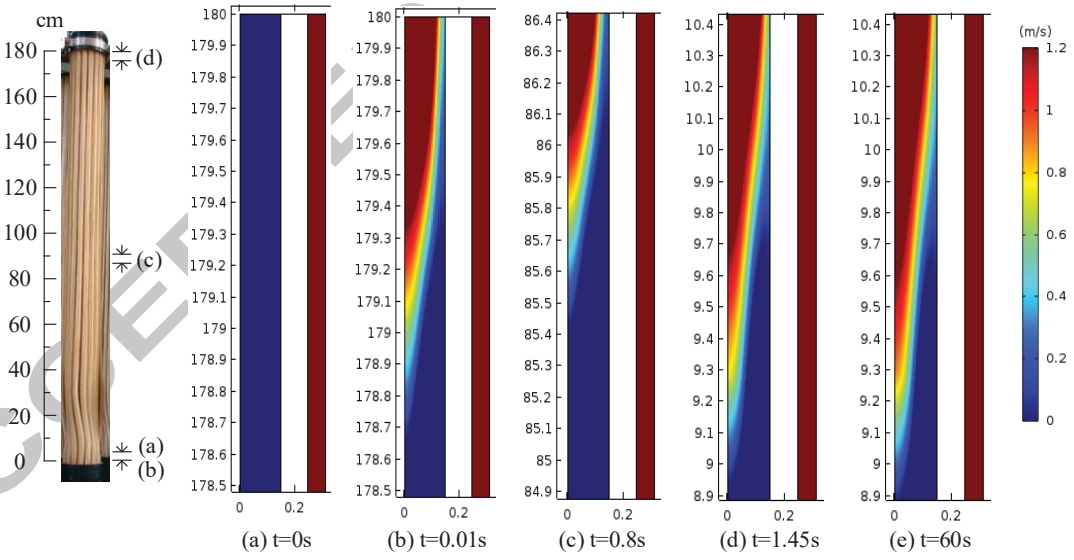

Fig. 5 Velocity variation inside fiber lumen at late membrane fouling stage

ACCEPTED MANUSCRIPT

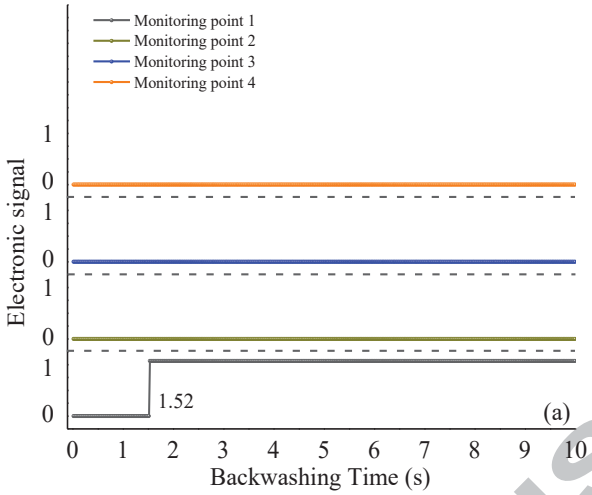

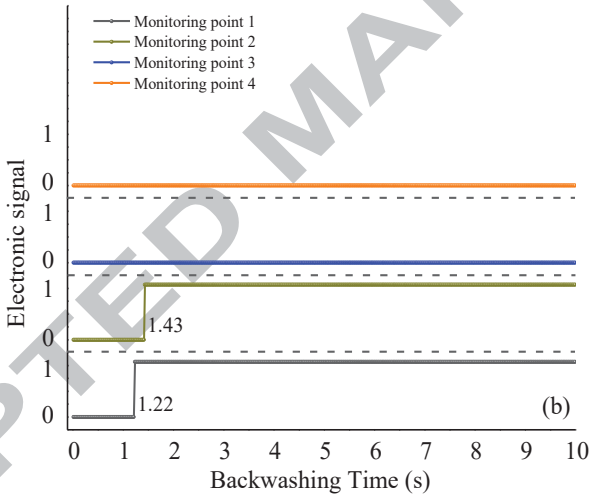

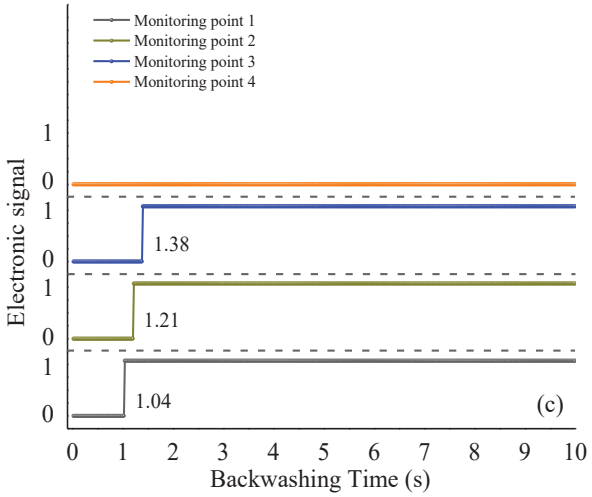

ACCEPTED MANUSCRIPT

Fig. 6 Signal variations of LBS for effective backwashing length: (a) Initial fouling stage; (b) Mid-term fouling stage; (c) Late fouling stage

ACCEPTED MANUSCRIPT

ACCEPTED MANUSCRIPT

Tab. 1 Boundary condition setting of flow field in dead-end backwashing

Boundary condition setting of flow field		
Boundary number	Boundary type	Settings
2	Pressure inlet	$P=P_0$
9	Pressure outlet	P=0
3	Wall	No slip
1	Symmetry	Symmetric boundary conditions

Tab. 2 Boundary condition setting of concentration field in dead-end backwashing

Boundary condition setting of flow field		
Boundary number	Boundary type	Settings
2	Inflow	$c=c_0$
4	Flux	$N=(1-m)*c*\vec{U}$
9	Outflow	Export boundary conditions
3	No flux	No flux boundary conditions
1	Symmetry	Symmetric boundary conditions

Tab. 3 Model parameters of hollow fiber membrane backwashing

Parameter	Value
Porosity (ε_p)	0.5
Permeability (K_{br})	3.34×10^{-16} m^2
Diffusion coefficient (D)	2.1×10^{-10} m^2/s
Foulants concentration (C)	5×10^4mg/L
Backwashing pressure (P_0)	0.1MPa
Retention rate (m)	97%
Membrane inner diameter (R_i)	0.03cm
Membrane outer diameter (R_o)	0.05cm
Membrane wire calculation domain radius (R)	0.065cm, 0.070cm, 0.075cm
Fiber length (L)	180cm

ACCEPTED MANUSCRIPT

Tab. 4 Settings of fouling level under simulated and experimental conditions

Fouling stages	Simulation parameter setting	Experimental parameter setting
Initial fouling stage (TMP=0~0.015MPa)	Fouling layer density =10000 mg/L	Backwashing began when TMP= 0.015Mpa
Mid-term fouling stage (TMP=0.015~0.05MPa)	Fouling layer density =15000 mg/L	Backwashing began when TMP=0.02Mpa
Late fouling stage (TMP≥0.05MPa)	Fouling layer density =50000 mg/L	Backwashing began when TMP=0.05Mpa

Tab. 5 Flux recovery rate at different fouling stages

Fouling stages	Effectiveness backwashing length	Flux recovery rate
Initial fouling stage (TMP=0.015MPa)	120cm	99.43%
Mid-term fouling stage (TMP=0.02MPa)	140cm	97.42%
Late fouling stage (TMP=0.05MPa)	160cm	82.29%

Tab. 6 Comparison of simulation and experimental results

Effective backwashing length	Backwash duration at different fouling stages								
	$R_f < R_m$			$Rf \geq Rm$			$Rf >> Rm$		
	V_s	V_e	σ	V_s	V_e	σ	V_s	V_e	σ
120cm	1.61s	1.52s	0.053	1.17s	1.22s	0.045	0.89s	1.017s	0.125
140cm	-	-		1.36s	1.43s	0.049	1.04s	1.186s	0.123
160cm	-	-		-	-	-	1.19s	1.356s	0.122
180cm	-	-	-	-	-	-	-	-	-

Note: V_s is for simulation data; V_e is for experimental data, σ is deviation.